Chiral separation and chiral magnetic effects in a slab: The role of boundaries

E. V. Gorbar,[1,2] V. A. Miransky,[3,4] I. A. Shovkovy,[5] and P. O. Sukhachov[1]

[1]*Department of Physics, Taras Shevchenko National Kiev University, Kiev 03680, Ukraine*
[2]*Bogolyubov Institute for Theoretical Physics, Kiev 03680, Ukraine*
[3]*Department of Applied Mathematics, Western University, London, Ontario N6A 5B7, Canada*
[4]*Department of Physics and Astronomy, Western University, London, Ontario N6A 3K7, Canada*
[5]*College of Letters and Sciences, Arizona State University, Mesa, Arizona 85212, USA*

We study the chiral separation and chiral magnetic effects in a slab of Dirac semimetal of finite thickness, placed in a constant magnetic field perpendicular to its surfaces. We utilize the Bogolyubov boundary conditions with a large Dirac mass (band gap) outside the slab. We find that, in a finite-thickness slab, the axial current density is induced by helicity-correlated standing waves and, as a consequence, is quantized. The quantization is seen in its stepped-shape dependence on the fermion chemical potential and a sawtooth-shape dependence on the thickness of the slab. In contrast to a naive expectation, there is no chiral charge accumulation anywhere in the bulk or at the boundaries of the semimetal. In the same slab geometry, we also find that a nonzero chiral chemical potential induces no electric current, as might have been expected from the chiral magnetic effect. We argue that this outcome is natural and points to the truly nonstatic nature of the latter. By taking into account a nonzero electric field of a double layer near the boundaries of the slab, we find that the low-energy modes under consideration satisfy the continuity equation for axial current density without the anomalous term.

I. INTRODUCTION

Nowadays there is significant interest in relativistic matter in a strong magnetic field. Such matter is intensively studied both experimentally and theoretically. It has a number of applications in high-energy physics and astrophysics (e.g., in the context of compact stars, heavy-ion collisions, and the early universe), as well as in condensed matter physics (e.g., in the context of novel Dirac/Weyl materials).

In condensed matter physics, after the first reports of three-dimensional Dirac semimetals appeared two years ago [1–3], the field exploded with numerous investigations of their exotic properties (for reviews, see Refs. [4–6]). One of the key aspects of such materials is a well-defined chirality of the low-energy quasiparticles, described by Weyl fermions. Because of the chiral anomaly [7], the chirality is not a conserved charge and, thus, the corresponding quasiparticles must come in both chiralities [8]. In Dirac semimetals, the low-energy spectra of the quasiparticles of opposite chiralities are degenerate. Such degeneracy is often protected by symmetries (e.g., the symmetry under time-reversal or parity). If the corresponding symmetry is broken, however, a Dirac semimetal may turn into a Weyl semimetal, in which the degeneracy of the quasiparticles with opposite chiralities is lifted. A number of materials of this latter type has been recently reported as well [9–15].

Phenomenologically, a chiral asymmetry in relativistic matter may be introduced via a nonzero chiral chemical potential μ_5 [16]. Such a chemical potential couples to a difference between the number densities of the left- and right-handed fermions and enters the Lagrangian density through the term $\mu_5 \bar{\psi} \gamma^0 \gamma^5 \psi$, where $\bar{\psi} \equiv \psi^\dagger \gamma^0$. The latter produces a chiral asymmetry in magnetized relativistic matter and leads to a nondissipative electric current $\mathbf{j} = e^2 \mathbf{B} \mu_5/(2\pi^2)$ in the presence of an external magnetic field $\mathbf{B}$ [16–18] (see also Refs. [19–22]). This phenomenon is known in the literature as the chiral magnetic effect (CME) and its origin is related to the famous chiral anomaly [7]. Moreover, the charge-dependent correlations and flow, observed in heavy-ion collisions at RHIC [23–27] and LHC [28], appear to be in a qualitative agreement with the predictions of the CME [29,30] (for recent reviews, see also Refs. [31–33]). In the context of condensed matter physics, it was also suggested that the measured quadratic field dependence of the magnetoconductance in $ZrTe_5$ is an indication of the chiral magnetic effect [34].

Unlike the chiral chemical potential, which is a rather exotic quantity and is not very well defined theoretically, the chemical potential μ (associated, for example, with a conserved electric or baryon charge) is common in many physical systems. It was shown in Refs. [35–37] that a nondissipative axial current density $\mathbf{j}_5 = -e\mathbf{B}\mu/(2\pi^2)$ exists in the equilibrium state of noninteracting massless fermion matter in a magnetic field. This effect is known as the chiral separation effect (CSE). In fact, as suggested in Refs. [38,39], the CSE may lead to a chiral charge separation (i.e., effectively inducing a nonzero chiral chemical potential μ_5) and, thus, trigger the CME even in the absence of topological fluctuations in the initial state.

The physical and mathematical reasons for the chiral asymmetry in relativistic matter in a magnetic field are quite transparent (for an elegant exposition, see also Ref. [40]). In essence, its origin is connected with the spin-polarized nature of the lowest Landau level (LLL). The corresponding fermionic states are also characterized by a well-defined longitudinal momentum and, thus, chirality. Moreover, the states with opposite signs of the longitudinal momenta carry opposite chiralities and, thus, lead to a nondissipative axial current density $\mathbf{j}_5 = -e\mathbf{B}\mu/(2\pi^2)$ [35,36].

It was argued in Refs. [36,37] that nondissipative currents in magnetized relativistic matter are determined by the topological currents induced exclusively in the LLL and are intimately connected with the chiral anomaly. This fact is

directly connected with the well-known result that the chiral anomaly in a magnetic field is also generated exclusively by the LLL [41]. The first studies of interaction effects on the chiral asymmetry of relativistic matter in a magnetic field were performed in Refs. [38,42,43] by using Nambu–Jona-Lasinio models with local interaction. In particular, it was found that the interaction unavoidably generates a chiral shift Δ [38,42] when the fermion density is nonzero. It enters the effective Lagrangian density through the following quadratic term: $\Delta \bar{\psi} \gamma^3 \gamma^5 \psi$, when the magnetic field is directed along the z direction. The meaning of the chiral shift parameter is most transparent in the chiral limit: it determines a relative shift of the longitudinal momenta in the dispersion relations of opposite chirality fermions, $k^3 \rightarrow k^3 \pm \Delta$, where the momentum k^3 is directed along the magnetic field. Furthermore, as shown in Refs. [38,42,44], the chiral shift Δ is responsible for an additional contribution to the axial current density. Also, such a dynamically generated chiral shift splits each Dirac node into a pair of Weyl nodes of opposite chirality, thus producing a Weyl semimetal from a Dirac one [45]. Recently, another interesting mechanism for inducing a nonzero chiral shift was proposed [46,47]. It uses a circularly polarized light and works even at zero chemical potential.

Usually the chiral magnetic and chiral separation effects are considered in the literature in unbounded material media. In practice, however, all physical systems (except for the CME and CSE in the early universe, perhaps) are finite. It is natural then to ask about the role of boundaries and finite-size effects in the chiral magnetic and separation effects. Indeed, even if one assumes that, in the bulk of a bounded medium, the electric and axial currents are the same as those in infinite systems, they should get modified near the boundaries. This should be an immediate consequence of the continuity equations if the currents are required to vanish outside the material. This simple observation was the main motivation for the present work. Here we will study the chiral separation and chiral magnetic effects in a slab with an external magnetic field perpendicular to the boundary planes of the slab, which yields the simplest realization of a finite-size system.

The paper is organized as follows. In Sec. II we introduce the model of a slab with the Bogolyubov boundary conditions [48], when the mass (band gap) parameter in the vacuum outside the slab is taken to be the largest mass (energy) parameter in the model. Note that we will use both the terms "mass" and "band gap" interchangeably throughout the paper. Section III is devoted to the analysis of the axial current density (i.e., the CSE) in the slab with such boundary conditions. The CME is considered in Sec. IV. In Sec. V we discuss the chiral anomaly in vacuum regions near the surface of the slab. The discussion of the main results is given in Sec. VI. Some technical details, including the derivation of the Landau-level wave functions and the implementation of the boundary conditions, are presented in Appendices A and B, respectively.

Throughout this paper, we set $\hbar = 1$ and $c = 1$.

II. MODEL

The Hamiltonian of the low-energy model of a Dirac semimetal slab situated between the planes $z = -a$ and $z = a$

reads

$$H = \int d^3\mathbf{r} \, \Psi^\dagger(\mathbf{r})[v_F \boldsymbol{\alpha} \cdot (-i\boldsymbol{\nabla} + e\mathbf{A}) + \gamma^0 m(z)]\Psi(\mathbf{r}), \quad (1)$$

where $\boldsymbol{\alpha} = \gamma^0 \boldsymbol{\gamma}$, and $\boldsymbol{\gamma}$ are the Dirac matrices in the chiral representation, i.e.,

$$\gamma^0 = \begin{pmatrix} 0 & -I_2 \\ -I_2 & 0 \end{pmatrix}, \quad \boldsymbol{\gamma} = \begin{pmatrix} 0 & \boldsymbol{\sigma} \\ -\boldsymbol{\sigma} & 0 \end{pmatrix},$$

$$\gamma^5 \equiv i\gamma^0\gamma^1\gamma^2\gamma^3 = \begin{pmatrix} I_2 & 0 \\ 0 & -I_2 \end{pmatrix}. \quad (2)$$

Here I_2 is the two-dimensional unit matrix and $\boldsymbol{\sigma} = (\sigma_1, \sigma_2, \sigma_3)$ are the Pauli matrices. By assuming that the external magnetic field $\mathbf{B}$ is directed along the z axis, we will find it convenient to use the vector potential in the Landau gauge, i.e., $\mathbf{A} = (0, Bx, 0)$. The other notations are as follows: e is the electron charge, v_F is the Fermi velocity, and $m(z) = M\theta(z^2 - a^2) + m\theta(a^2 - z^2)$ is the Dirac mass (band gap) function [here $\theta(x)$ is the unit step function]. The case of a Dirac semimetal with a zero band gap in the bulk is obtained by taking the limit $m \rightarrow 0$. In the model at hand, we assume that the "vacuum" gap parameter M is much larger than all characteristic energy scales in the slab (e.g., the work function and/or relevant quasiparticle energies). Interestingly, such a model of the slab is nothing else but a generalized Bogolyubov bag model [48]. In the studies of graphene, similar boundary conditions with an infinite gap outside the material are known as the infinite mass boundary conditions [49,50]. The same idea, albeit with a finite-size band gap, is also utilized in modeling a potential barrier in the context of the Klein paradox in graphene; see Ref. [51]. While $m = 0$ was used in the original Bogolyubov model, we will treat m as a free parameter in the analysis below. (Note that the $m \neq 0$ case is of interest not only from a theoretical viewpoint, but could be also investigated experimentally in a more general class of Dirac semimetals/metals, e.g., such as a bismuth alloy $Bi_{1-x}Sb_x$ at small concentrations of antimony [52,53], where the Dirac gap is nonzero.) For a good review of bag models in hadron physics, see Ref. [54]. Generically, in all such models, the hadrons are described as bags with massless fermions (quarks) confined inside. In order to prevent massless fermions from leaving the bag, one requires that the normal components of the momenta and hence the currents across the surface vanish. Such boundary conditions necessarily break the chiral symmetry for fermions [54]. From the physics viewpoint, this is unavoidable because massless quasiparticles experience a helicity flip (and, thus, a chirality change) whenever the directions of their momenta change due to scattering from the boundary. This fact will be crucial for our analysis below. In particular, in the Bogolyubov model with the vanishing gap in the bulk, $m \rightarrow 0$, the chiral symmetry is explicitly broken by the inclusion of the (infinitely) large vacuum gap parameter M.

III. CHIRAL SEPARATION EFFECT

In this section, we calculate the axial current density and study the CSE in a Dirac semimetal with a slab geometry. By making use of Hamiltonian (1), the ground state of the

system will be obtained by filling all quasiparticle states with the energies less than the Fermi energy $E_F = \mu$, where μ is the chemical potential.

Let us start by determining the energy spectrum and the electron wave functions for a Dirac semimetal slab in

a constant magnetic field. Before proceeding to the slab case, however, it is instructive to start from presenting the Landau-level wave functions in an infinite space. By making use of the chiral representation (2), we derive the following results for the wave functions (see Appendix A for details):

$$\psi(\mathbf{r})_{n=0} = C_0 \, e^{ip_z z + ip_y y} \begin{pmatrix} 0 \\ Y_0(\xi) \\ 0 \\ -\frac{m}{E_0 - v_F p_z} Y_0(\xi) \end{pmatrix}, \tag{3}$$

$$\psi(\mathbf{r})_{n>0} = e^{ip_z z + ip_y y} \left[C_+ \begin{pmatrix} -i\frac{m^2 + 2n\epsilon_L^2}{(E_n - v_F p_z)\sqrt{2n\epsilon_L^2}} Y_{n-1}(\xi) \\ Y_n(\xi) \\ i\frac{m}{\sqrt{2n\epsilon_L^2}} Y_{n-1}(\xi) \\ 0 \end{pmatrix} + C_- \begin{pmatrix} -i\frac{m\sqrt{m^2 + 2n\epsilon_L^2}}{(E_n - v_F p_z)\sqrt{2n\epsilon_L^2}} Y_{n-1}(\xi) \\ 0 \\ i\frac{\sqrt{m^2 + 2n\epsilon_L^2}}{\sqrt{2n\epsilon_L^2}} Y_{n-1}(\xi) \\ \frac{\sqrt{m^2 + 2n\epsilon_L^2}}{E_n - v_F p_z} Y_n(\xi) \end{pmatrix} \right], \tag{4}$$

where $l = 1/\sqrt{|eB|}$ is the magnetic length, $\epsilon_L = v_F\sqrt{eB}$ is the Landau energy scale, and $\xi = x/l + p_y l$. For convenience, here, we fixed the sign of electric charge so that $\mathrm{sgn}(eB) = +1$. Additionally, we introduced the following harmonic oscillator wave functions: $Y_n(\xi) = \frac{e^{-\xi^2/2}}{\sqrt{2^n n! \sqrt{\pi}}} H_n(\xi)$, where $H_n(\xi)$ are the Hermite polynomials. (For the Landau-level wave functions in the standard representation of the Dirac matrices, see Ref. [55].) The corresponding Landau-level energies are given by $E_n = \pm\sqrt{v_F^2 p_z^2 + m^2 + 2n\epsilon_L^2}$.

Now, in the case of a slab with a finite extent in the z direction, for every plane wave with a wave vector p_z, propagating in the positive z direction, there should be also a plane wave with a wave vector $-p_z$, propagating in the opposite direction. Therefore, the general solution for the nth-Landau-level wave function in the slab is given by a superposition of two counterpropagating plane waves, or equivalently, a standing wave:

$$\Psi_{\mathrm{slab}}(\mathbf{r})_{n=0} = C_0 \, e^{ip_z z + ip_y y} \begin{pmatrix} 0 \\ Y_0(\xi) \\ 0 \\ -\frac{m}{E_0 - v_F p_z} Y_0(\xi) \end{pmatrix} + \tilde{C}_0 \, e^{-ip_z z + ip_y y} \begin{pmatrix} 0 \\ Y_0(\xi) \\ 0 \\ -\frac{m}{E_0 + v_F p_z} Y_0(\xi) \end{pmatrix}, \tag{5}$$

$$\Psi_{\mathrm{slab}}(\mathbf{r})_{n>0} = e^{ip_z z + ip_y y} \left[C_+ \begin{pmatrix} -i\frac{m^2 + 2n\epsilon_L^2}{(E_n - v_F p_z)\sqrt{2n\epsilon_L^2}} Y_{n-1}(\xi) \\ Y_n(\xi) \\ i\frac{m}{\sqrt{2n\epsilon_L^2}} Y_{n-1}(\xi) \\ 0 \end{pmatrix} + C_- \begin{pmatrix} -i\frac{m\sqrt{m^2 + 2n\epsilon_L^2}}{(E_n - v_F p_z)\sqrt{2n\epsilon_L^2}} Y_{n-1}(\xi) \\ 0 \\ i\frac{\sqrt{m^2 + 2n\epsilon_L^2}}{\sqrt{2n\epsilon_L^2}} Y_{n-1}(\xi) \\ \frac{\sqrt{m^2 + 2n\epsilon_L^2}}{E_n - v_F p_z} Y_n(\xi) \end{pmatrix} \right] + (p_z \to -p_z, C_\pm \to \tilde{C}_\pm).$$

$$\tag{6}$$

These wave functions inside the slab should be matched to the corresponding solutions in the vacuum. This is done in Appendix B using the Bogolyubov bag model, in which wave functions outside the semimetal satisfy the Dirac equation with an infinitely large vacuum gap parameter M. By enforcing the boundary conditions, we also find that the wave vector p_z should satisfy the following spectral equation:

$$v_F p_z \cos(2ap_z) + m \sin(2ap_z) = 0, \tag{7}$$

where $p_z \neq 0$. The final expressions for the Landau-level wave functions in the slab are given in Eqs. (B7), (B15), and (B16). In essence, they have the form of standing waves with discrete wave vectors p_z that satisfy Eq. (7). It is important to note that, while there are two independent solutions for each wave vector in the higher Landau levels, there is only one independent solution for each wave vector in the LLL.

A. Axial current density

In this subsection, we calculate the axial current density inside the slab. In terms of the Landau-level wave functions, the corresponding ground-state expectation value is given by

$$\langle j_5^3 \rangle = \int \frac{dp_y}{2\pi} \sum_{p_z} \left(f(p_z) \, v_F \Psi_{\mathrm{slab}}^\dagger(\mathbf{r})_{n=0} \gamma^0 \gamma^3 \gamma^5 \Psi_{\mathrm{slab}}(\mathbf{r})_{n=0} \right.$$
$$\left. + \sum_{i=1}^{2} \sum_{n=1}^{\infty} f(p_z) \, v_F \Psi_{\mathrm{slab}}^{(i)\dagger}(\mathbf{r})_n \gamma^0 \gamma^3 \gamma^5 \Psi_{\mathrm{slab}}^{(i)}(\mathbf{r})_n \right), \tag{8}$$

where the contributions of quasiparticles from both valence and conduction bands are taken into account via the use of the

following generalized distribution function:

$$f(p_z) = \frac{1}{e^{(\sqrt{v_F^2 p_z^2 + m^2 + 2n\epsilon_L^2} - \mu)/T} + 1}$$
$$- \frac{1}{e^{(\sqrt{v_F^2 p_z^2 + m^2 + 2n\epsilon_L^2} + \mu)/T} + 1}. \quad (9)$$

Here μ is the chemical potential (Fermi energy) measured from the Dirac point. This distribution function accounts for the fact that the quasiparticles of the conduction and valence bands carry opposite charges. In the zero-temperature limit, which we use in the following, this function simplifies:

$$\lim_{T \to 0} f(p_z) = \mathrm{sgn}(\mu)\theta\big(\mu^2 - v_F^2 p_z^2 - m^2 - 2n\epsilon_L^2\big), \quad (10)$$

where $\theta(x)$ is the unit step function.

When calculating the axial current density, it is instructive to separate the contribution of the spin-polarized lowest Landau level from the contributions of the higher Landau levels ($n > 0$). The LLL contribution is obtained by making use of the wave function in Eq. (B7). The zero-temperature result reads

$$\langle j_5^3 \rangle_{n=0} = \int \frac{dp_y}{2\pi} \sum_{p_z} f(p_z)\, v_F \Psi_{\mathrm{slab}}^{\dagger}(\mathbf{r})_{n=0} \gamma^0 \gamma^3 \gamma^5 \Psi_{\mathrm{slab}}(\mathbf{r})_{n=0}$$
$$= -\frac{eB v_F \,\mathrm{sgn}(\mu)}{2a\pi} \sum_{p_z} \theta\big(\mu^2 - v_F^2 p_z^2 - m^2\big)$$
$$\times \frac{\big(m^2 + v_F^2 p_z^2\big)[1 - \cos(2p_z z)\cos(2p_z a)]}{2\big(m^2 + v_F^2 p_z^2\big) + m v_F/a}, \quad (11)$$

where we also made use of the spectral equation in Eq. (7). As we see, in a general case when $m \neq 0$, the LLL contribution to the axial current density has a nontrivial dependence on the z coordinate. Here it may be appropriate to mention that the axial current density is well defined even in the gapped case when the axial charge is not conserved. In fact, even in the extreme nonrelativistic limit, it has a clear physical meaning as a spin polarization.

As expected, in the chiral (gapless) limit, the axial current density is independent of the z coordinate and the explicit result reads

$$\langle j_5^3 \rangle_{n=0, m \to 0} = -\frac{eB v_F \,\mathrm{sgn}(\mu)}{4a\pi} \sum_{p_z} \theta\big(\mu^2 - v_F^2 p_z^2\big)$$
$$= -\frac{eB v_F \,\mathrm{sgn}(\mu)}{4a\pi} k_{\max}, \quad (12)$$

where we took into account the spectral equation (7), which reduces down to $\cos(2ap_z) = 0$ in the gapless case. The latter also implies that the allowed values of the wave vector are $p_{z,k}^{(0)} = (2k-1)\pi/(4a)$, where k is a positive integer. Because of the unit step function in Eq. (12), the result of the sum is given by $k_{\max} = [2a|\mu|/(v_F\pi) + 1/2]$ where $[\ldots]$ represents the integer part. As expected, in the limit of $a \to \infty$, the above result reduces to the well-known relation for the chiral separation effect in an infinite system, i.e., $\langle j_5^3 \rangle = -|eB|\mu/(2\pi^2)$.

The result in Eq. (12) shows that, in a slab of finite thickness a, the axial current density is quantized. This is a qualitatively new feature that did not exist in an infinite system. It is a

natural outcome of having the wave functions in the form of standing waves and the quantization of the wave vector in a slab geometry. As is easy to see from Eq. (12), the height of the steps in the axial current is proportional to the magnetic field and inversely proportional to the thickness of the slab, i.e., $\delta\langle j_5^3 \rangle = eB v_F/(4a\pi)$. When $\langle j_5^3 \rangle$ is plotted as a function of $a\mu/v_F$, the widths of the steps are given by $\pi/2$. It would be interesting to explore whether such a quantization can be observed in experiment.

In the case of higher Landau levels ($n > 0$), there are separate contributions to the axial current density from each of the two independent modes in the slab, i.e., $\Psi_{\mathrm{slab}}^{(1)}(\mathbf{r})_n$ and $\Psi_{\mathrm{slab}}^{(2)}(\mathbf{r})_n$. By making use of the explicit expressions for the corresponding wave functions in Eqs. (B15) and (B16), we find that, for each p_z, the two contributions have opposite signs, i.e.,

$$\int \frac{dp_y}{2\pi} v_F \Psi_{\mathrm{slab}}^{(1)\dagger}(\mathbf{r})_n \gamma^0 \gamma^3 \gamma^5 \Psi_{\mathrm{slab}}^{(1)}(\mathbf{r})_n$$
$$= -\frac{eB}{2\pi} \frac{v_F p_z\big(m^2 + v_F^2 p_z^2\big)[1 - \cos(2p_z z)\cos(2p_z a)]}{2ap_z E_n^2 + v_F p_z m - n\epsilon_L^2 \sin(4ap_z)}, \quad (13)$$

$$\int \frac{dp_y}{2\pi} v_F \Psi_{\mathrm{slab}}^{(2)\dagger}(\mathbf{r})_n \gamma^0 \gamma^3 \gamma^5 \Psi_{\mathrm{slab}}^{(2)}(\mathbf{r})_n$$
$$= \frac{eB}{2\pi} \frac{v_F p_z\big(m^2 + v_F^2 p_z^2\big)[1 - \cos(2p_z z)\cos(2p_z a)]}{2ap_z E_n^2 + v_F p_z m - n\epsilon_L^2 \sin(4ap_z)}. \quad (14)$$

Therefore, there is no net contribution to the axial current density due to higher Landau levels. In other words, just like in the case of an infinite space [36], the axial current density in a semimetal slab is determined exclusively by the LLL contribution (11).

Our numerical results for the axial current density (11) in a slab geometry are presented in Figs. 1, 2, and 3. For comparison, in Figs. 1 and 2 we also show the results for an infinite space. The dependence of the dimensionless axial current density $2\pi^2 \langle j_5^3 \rangle al^2/v_F$, in the middle of the slab ($z = 0$), as a function of the chemical potential is presented in Fig. 1. [Recall that the axial current density in Eq. (11) is not uniform in space when $m \neq 0$.] The three panels show the results for three representative values of the band gap: $am/v_F = 0$ (left panel), $am/v_F = 2$ (middle panel), and $am/v_F = 6$ (right panel). To plot the figure, we used $v_F/a = 25$ meV. As expected, a nonzero current density is obtained only when $\mu > m$, i.e., when the chemical potential is larger than the size of the band gap. In agreement with the earlier observation, we also see that the axial current density is quantized in the slab.

The dependence of the dimensionless axial current density $2\pi^2 \langle j_5^3 \rangle l^2/\mu$, in the middle of the slab ($z = 0$), as a function of the width is shown in Fig. 2. The three panels show the results for the following three values of the band gap: $m/\mu = 0$ (left panel), $m/\mu = 0.25$ (middle panel), and $m/\mu = 0.75$ (right panel). To plot the figure, we used $v_F/\mu = 12.5$ Å. As we find, the functional dependence of the current density on the width of the slab has a sawtooth shape. This is rather
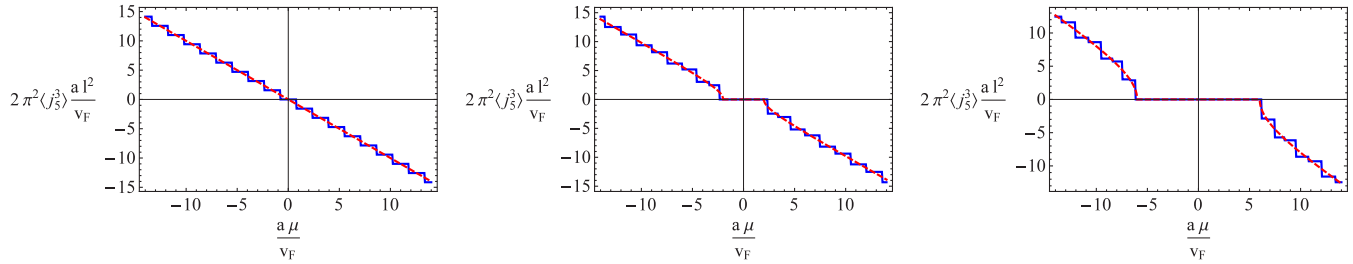
FIG. 1. (Color online) The dimensionless axial current density in an infinite space (red dashed line) and in the middle of the slab (blue solid line) plotted as a function of chemical potential for the three values of the band gap: $am/v_F = 0$ (left panel), $am/v_F = 2$ (middle panel), and $am/v_F = 6$ (right panel). To plot the figure, we fixed $v_F/a = 25$ meV.

natural consequence of the quantization of the wave vector. When the size a becomes large, the finite-size effects quickly decrease and the result approaches the limit of an infinite system. We also see that a nonzero gap has a damping effect in the dependence on a. (Notice the difference in the vertical scales in the three panels of Fig. 2.)

It is interesting to note that, in the gapped case ($m \neq 0$), the steps in the axial current density have different heights; see Fig. 1. This is pronounced the most in the lowest few steps of the current density. (Note, at the same time, that the widths of the steps in $a\mu/v_F$ remain nearly, although not exactly, the same.) The corresponding steps are determined by the low-energy quasiparticle states with the smallest few wave vectors, i.e., the wave vectors which are modified the most by a nonzero gap. This can be checked explicitly in the limit of a small but nonzero band gap. In such a limit, an analytical expression for the wave vectors can be obtained approximately by solving the spectral equation (7). The result reads $p_{z,k}^{(m)} \simeq (2k-1)\pi/(4a) + 2m/[\pi v_F(2k-1)]$ where k is a positive integer. By making use of this, one can check that the contributions from the states with small k vary a lot because of great variations in the values of $\cos(2p_{z,k}^{(m)}a)$; see Eq. (11). (Away from the middle point in the slab, the heights of the steps also vary. This is clear from Fig. 3.) With increasing the value of $a|\mu|/v_F$, on the other hand, the effect of the gap diminishes and the functional dependence of the axial current density gradually approaches the result in the gapless limit. This is understandable since the states with large wave vectors, which dominate the result in such a regime, are insensitive to the size of the gap.

As is clear from Eq. (11), in the case of a nonzero band gap, the axial current density is not uniform: it depends

on the position z inside the semimetal. The corresponding dependence is shown explicitly in Fig. 3, where we present the results for the gapless case $am/v_F = 0$ (left panel) alongside the results for the two cases with nonzero band gaps: $am/v_F = 2$ (middle panel) and $am/v_F = 6$ (right panel). The fact that the axial current density is constant inside the slab in the gapless case is consistent with the continuity equation. Indeed, in the case of the vanishing gap and in the absence of electric fields, the axial current is conserved inside the slab. In contrast, there are clearly visible oscillations of the axial current density in the other two cases when $m \neq 0$ (see the middle and right panels in Fig. 3). Taking into account that the axial current is not conserved in the gapped case, such oscillations are not forbidden. Moreover, as we see, the larger is the gap, the more pronounced are the oscillations. When the gap is fixed, we also find that the local amplitude of the axial current density oscillations is not the same across the whole sample: it decreases with the increasing distance from the slab boundaries.

It may be interesting to emphasize that, in a finite-thickness slab, the axial current density originates from helicity-correlated standing waves. Of course, the underlying roots of this are (i) finite thickness of the slab and (ii) the spin-polarized nature of the LLL. This can be seen explicitly from the structure of the LLL wave function in Eq. (B7), which takes the following simple form in the gapless limit:

$$\Psi_{\text{slab}}(\mathbf{r})_{n=0} = -\frac{e^{ip_y y - (lp_y + x/l)^2/2}}{2\pi^{1/4}\sqrt{al}} \begin{pmatrix} 0 \\ i e^{2iap_z - ip_z z} \\ 0 \\ e^{ip_z z} \end{pmatrix}. \quad (15)$$
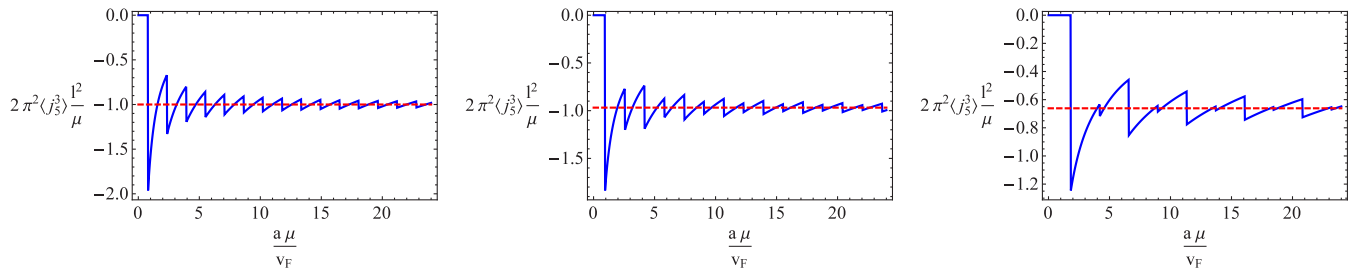

FIG. 2. (Color online) The dimensionless axial current density in an infinite space (red dashed line) and in the middle of the slab (blue solid line) plotted as a function of the width of the slab a for the three values of the band gap: $m/\mu = 0$ (left panel), $m/\mu = 0.25$ (middle panel), and $m/\mu = 0.75$ (right panel). To plot the figure, we fixed $v_F/\mu = 12.5$ Å.
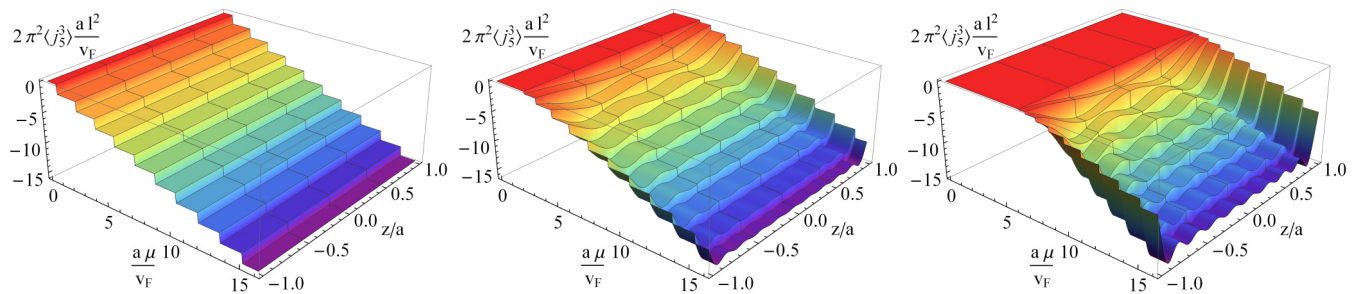
FIG. 3. (Color online) The dimensionless axial current density plotted as a function of the chemical potential and z/a for the three values of the band gap: $am/v_F = 0$ (left panel), $am/v_F = 2$ (middle panel), and $am/v_F = 6$ (right panel). To plot the figure, we fixed $v_F/a = 25$ meV.

Such a standing wave is made of a pair of counterpropagating plane waves carrying opposite chiralities or helicities. This is clear since, in the chiral representation used, see Eq. (2), the upper (lower) two components of the wave function describe right-handed (left-handed) modes. The configuration in Eq. (15) can be interpreted as follows: the helicity of each plane wave propagating to the boundary flips the sign after the reflection. This is indeed expected for the spin-polarized LLL states. A nontrivial helicity correlation of the LLL standing waves remains even in the gapped case, but it is not as transparent. Such a correlation is the key feature that is responsible for the axial current density in a semimetal slab.

Before concluding this subsection, let us briefly discuss the implications of the chiral separation effect in a slab of finite thickness. Naively, one may expect that the axial current density in the bulk of the semimetal should lead to an accumulation of positive chiral charge on one side of the slab, and negative chiral charge on the other. As is easy to check, however, this does not occur. In fact, the axial charge density is identically zero everywhere, $\langle j_5^0 \rangle \equiv 0$.

B. Axial current in the vacuum with finite band gap

As the results in the previous subsection show, in a slab geometry, there is a nonzero axial current density in the bulk

of semimetal. However, the current should be vanishing in the vacuum because of the imposed boundary conditions. Then, the current density should presumably go to zero in the surface layer. In order to clarify this issue, in this subsection, we investigate the continuity equation for the axial current density at the vacuum side of the slab.

In the absence of an electric field, the axial charge and current densities should satisfy the following continuity equation [7]:

$$\partial_0 j_5^0 + \nabla \cdot \mathbf{j}_5 = 2m(z) i \psi^\dagger \gamma^0 \gamma^5 \psi, \qquad (16)$$

in all regions of space, including at the boundary of the slab. Note that, in order to have the continuity equation well defined, we will assume that the vacuum band gap M is large, but finite. The corresponding results for the LLL wave functions are derived in Appendix B 3; see Eqs. (B22), (B23), and (B24). Also, in the same Appendix, we derive a modified version of the spectral equation for the wave vector p_z; see Eq. (B21).

By making use of the wave functions in Eqs. (B23) and (B24), we can also compute the axial current density outside the slab. In the region $z > a$, the corresponding result is given by

$$\langle j_5^3 \rangle_{n=0,z>a} = -\frac{|eB| v_F \operatorname{sgn}(\mu)}{2\pi a} \sum_{p_z} \theta\left(\mu^2 - v_F^2 p_z^2 - m^2\right)$$

$$\times \frac{v_F^2 p_z^2 M e^{-2(z-a)\sqrt{M^2 - v_F^2 p_z^2 - m^2}/v_F}}{2\left(v_F^2 p_z^2 + m^2\right)(M - m) + \frac{m v_F \sqrt{M^2 - \left(v_F^2 p_z^2 + m^2\right)}}{a} + \frac{v_F^3 p_z^2 M}{a\sqrt{M^2 - \left(v_F^2 p_z^2 + m^2\right)}}}, \qquad (17)$$

where the sum is performed over the discrete values of the wave vectors that satisfy Eq. (B21). The result in the region $z < -a$ is similar, but one should replace $-(z-a) \rightarrow (z+a)$.

In order to check the continuity equation in the regions outside the slab, let us calculate the ground-state expectation value of the quantity that appears on right-hand side of Eq. (16). It is straightforward to show that

$$2i M \langle \psi^\dagger_{z>a} \gamma^0 \gamma^5 \psi_{z>a} \rangle = \frac{|eB| \operatorname{sgn}(\mu)}{2\pi a} \sum_{p_z} \theta\left(\mu^2 - v_F^2 p_z^2 - m^2\right) 2\sqrt{M^2 - v_F^2 p_z^2 - m^2}$$

$$\times \frac{v_F^2 p_z^2 M e^{-2(z-a)\sqrt{M^2 - v_F^2 p_z^2 - m^2}/v_F}}{2\left(v_F^2 p_z^2 + m^2\right)(M - m) + \frac{m v_F \sqrt{M^2 - \left(v_F^2 p_z^2 + m^2\right)}}{a} + \frac{v_F^3 p_z^2 M}{a\sqrt{M^2 - \left(v_F^2 p_z^2 + m^2\right)}}}. \qquad (18)$$

In the region $z < -a$, the corresponding quantity is obtained by replacing $-(z - a) \to (z + a)$ and flipping the overall sign.

By taking the derivative of Eq. (17) with respect to z and making use of Eq. (18), we check that the continuity equation (16) is indeed satisfied in the regions outside the slab. Therefore, the axial current flows to the boundary, where, due to the presence of the large vacuum mass M, it exponentially vanishes. Moreover, as claimed earlier, this happens without any chiral charge accumulation at the boundaries.

IV. CHIRAL MAGNETIC EFFECT IN THE SLAB

In this section, we will study the chiral magnetic effect in a slab geometry (for simplicity, only the case of the chiral limit will be considered here). In order to do this, we need to introduce a nonzero chiral chemical potential μ_5 into our model of a semimetal. In the chiral limit, one might try to introduce μ_5 by just replacing the fermion number chemical potential μ with $\mu \pm \mu_5$ in the distribution function (10) for the right- and left-handed particles, respectively. By recalling, however, that in the presence of the boundaries the chiral symmetry is broken even in the case of gapless Dirac fermions in the bulk, we know that μ_5 does not correspond to a conserved quantity. In such a situation, it is more convenient to treat μ_5 as a phenomenological parameter that modifies the model Hamiltonian, i.e.,

$$H = \int d^3\mathbf{r}\, \Psi^\dagger(\mathbf{r})[v_F \boldsymbol{\alpha} \cdot (-i\boldsymbol{\nabla} + e\mathbf{A}) - \mu - \mu_5\gamma^5]\Psi(\mathbf{r}). \tag{19}$$

It is worth noting that in the model under consideration μ_5 determines the relative energy shift of the left- and right-handed Weyl nodes. We calculate the ground-state expectation values by using the Schwinger prescription, where the summation over energy eigenvalues is performed with the distribution function $f_0(E) = -\text{sgn}(E)/2$. [Note that, in this case, the effective distribution function $f_0(E_-) + f_0(E_+)$, where $E_\pm = -\mu \pm \sqrt{v_F^2 p_z^2 + 2n\epsilon_L^2}$, gives the same distribution as Eq. (10) in the gapless limit.]

For Hamiltonian (19), we find the following LLL wave function inside the semimetal:

$$\Psi_{\text{slab}}(\mathbf{r})_{n=0} = Y_0(\xi)e^{ip_y y}\left\{ e^{ip_z z}C_0\begin{pmatrix}0\\1\\0\\0\end{pmatrix} + e^{i\tilde{p}_z z}\tilde{C}_0\begin{pmatrix}0\\0\\0\\1\end{pmatrix}\right\}, \tag{20}$$

where $p_z = -(E + \mu + \mu_5)/v_F$ and $\tilde{p}_z = (E + \mu - \mu_5)/v_F$. The corresponding wave functions outside the slab are given by Eqs. (B1) and (B2). By making use of the matching conditions in Eqs. (B3) and (B4), we derive the spectral equation for the wave vectors, $\cos[a(p_z - \tilde{p}_z)] = 0$. By solving this equation, we find that the energy parameter E can take only the following discrete values:

$$E_k = -\mu + \frac{\pi v_F}{2a}\left(k - \frac{1}{2}\right), \tag{21}$$

where k is a positive integer. After enforcing the boundary conditions, we also derive the following final expression for the wave function inside the slab:

$$\Psi_{\text{slab}}(\mathbf{r})_{n=0} = \frac{Y_0(\xi)e^{ip_y y}}{2\sqrt{al}}\begin{pmatrix}0\\e^{ip_z z}\\0\\-ie^{ip_z a + i\tilde{p}_z(z-a)}\end{pmatrix}, \tag{22}$$

and find that the corresponding LLL contribution to the electric current vanishes,

$$\langle j^3 \rangle = \sum_{k=1}^{\infty} f(E_k)v_F\Psi_{\text{slab}}^\dagger(\mathbf{r})_{n=0}\gamma^0\gamma^3\Psi_{\text{slab}}(\mathbf{r})_{n=0} = 0. \tag{23}$$

Although this result is natural in the Bogolyubov model, it may appear surprising because it is precisely the LLL contribution that saturates the CME in an infinite system. To complete the analysis of the CME in a finite slab, however, we should still analyze the contributions of higher Landau levels ($n > 0$). For a semimetal described by Hamiltonian (19), the wave functions in higher Landau levels are given by

$$\Psi_{\text{slab}}(\mathbf{r})_n = e^{ip_y y}\left[C_1 e^{iP_z z}\begin{pmatrix}-iv_F\left(\sqrt{P_z^2 + \frac{2n\epsilon_L^2}{v_F^2}} + P_z\right)Y_{n-1}(\xi)\\ \sqrt{2n\epsilon_L^2}\,Y_n(\xi)\\0\\0\end{pmatrix} + C_2 e^{i\tilde{P}_z z}\begin{pmatrix}0\\0\\iv_F\left(\sqrt{\tilde{P}_z^2 + \frac{2n\epsilon_L^2}{v_F^2}} - \tilde{P}_z\right)Y_{n-1}(\xi)\\ \sqrt{2n\epsilon_L^2}\,Y_n(\xi)\end{pmatrix}\right.$$
$$\left. + C_3 e^{-iP_z z}\begin{pmatrix}-iv_F\left(\sqrt{P_z^2 + \frac{2n\epsilon_L^2}{v_F^2}} - P_z\right)Y_{n-1}(\xi)\\ \sqrt{2n\epsilon_L^2}\,Y_n(\xi)\\0\\0\end{pmatrix} + C_4 e^{-i\tilde{P}_z z}\begin{pmatrix}0\\0\\iv_F\left(\sqrt{\tilde{P}_z^2 + \frac{2n\epsilon_L^2}{v_F^2}} + \tilde{P}_z\right)Y_{n-1}(\xi)\\ \sqrt{2n\epsilon_L^2}\,Y_n(\xi)\end{pmatrix}\right], \tag{24}$$

where $P_z = v_F^{-1}\sqrt{(E + \mu + \mu_5)^2 - 2n\epsilon_L^2}$ and $\tilde{P}_z = v_F^{-1}\sqrt{(E + \mu - \mu_5)^2 - 2n\epsilon_L^2}$.

The corresponding spectral equation is obtained by matching the wave functions in the bulk with those in the vacuum; see Eqs. (B3) and (B4). Its explicit form reads

$$(1 - e^{4iaP_z})(1 - e^{4ia\tilde{P}_z})\left[(E + \mu)^2 - \mu_5^2 - 2n\epsilon_L^2\right] + v_F^2 P_z\tilde{P}_z(1 + e^{4iaP_z} + e^{4ia\tilde{P}_z} + 4e^{2ia(P_z + \tilde{P}_z)} + e^{4ia(P_z + \tilde{P}_z)}) = 0. \tag{25}$$

When $\mu_5 \neq 0$, we could solve this equation only numerically. By making use of the spectral equation, we can write down the formal solution for the semimetal wave function in the slab. The corresponding expression is bulky and not very informative. Therefore, we do not present it here. Instead, by making use of the numerical solutions to Eq. (25), we calculate the contribution of the higher Landau levels to the electric and axial current densities. Both results vanish within the numerical precision used.

Thus, unlike the axial current density of the CSE, the electric current density of the CME is absent in the slab. This result might have been expected from general considerations. Because of the Bogolyubov bag model boundary conditions (with an infinite band gap in vacuum), there should be no electric current across the boundary. Taking into account that the electric current is not anomalous, this means that the continuity equation for the electric current can be satisfied only if the electric current vanishes inside the slab. This is exactly what the direct calculations give. Moreover, in the model at hand, the electric current will remain vanishing even in the limit $a \to \infty$. This fact is consistent with the case of infinite systems in equilibrium considered in Refs. [56–58].

In passing, let us briefly discuss the simplest case of a Weyl semimetal. The corresponding model Hamiltonian will be similar to that in Eq. (19), but will include an additional term, $-v_F \int d^3\mathbf{r}\, \Psi^\dagger(\mathbf{r})(\boldsymbol{\alpha} \cdot \boldsymbol{\Delta})\gamma^5 \Psi(\mathbf{r})$. The value of $\boldsymbol{\Delta} \equiv \Delta \mathbf{e}_z$, which is often called the chiral shift parameter, determines the separation between the Weyl nodes in momentum space. Here, for simplicity, we assume that $\boldsymbol{\Delta}$ points in the $+z$ direction. This may be sufficient because the components of the chiral shift parallel to the slab surface are not expected to modify the currents in the slab. When $\Delta \neq 0$, we find that the LLL wave functions in the bulk have the same form as in Eq. (20), but with $p_z = -(E + \mu + \mu_5)/v_F + \Delta$ and $\tilde{p}_z = (E + \mu - \mu_5)/v_F - \Delta$. Then, by making use of the wave functions outside the slab, see Eqs. (B1) and (B2), and enforcing the boundary conditions in Eqs. (B3) and (B4), we find that the energy can take only the following discrete values:

$$E_k = -\mu + v_F \Delta + \frac{\pi v_F}{2a}\left(k - \frac{1}{2}\right), \quad (26)$$

where k is a positive integer. Compared to the result in Eq. (21), the only difference here is the change $\mu \to \mu - v_F \Delta$. This finding is in agreement with the result in an infinite system, obtained in Ref. [42]. The calculation of the higher Landau level contributions to the axial current is more challenging in the general case $\mu_5 \neq 0$. Therefore, we restrict our discussion to the simpler case, $\mu_5 = 0$. In contrast to the case of an infinite system, we find that the contributions of higher Landau levels to the axial current density vanish. Therefore, our results for the axial and electric current densities in a Dirac semimetal slab, see Eqs. (12) and (23), remain qualitatively the same also in the case of a Weyl semimetal slab, but with the replacement $\mu \to \mu - v_F \Delta$.

V. WORK FUNCTION, ELECTRIC FIELDS, AND CONTINUITY EQUATION FOR AXIAL CURRENT

The work function of a solid is defined as the energy needed to remove an electron from the solid to vacuum (see,

e.g., [59]). Microscopically, it can be thought of as the result of a "confining" electric field $\boldsymbol{\mathcal{E}}$ near the surface, resulting from the electron density leaking slightly out of the material. In the problem at hand, we consider a semimetal slab with a nonzero magnetic field perpendicular to its surface. This means that $\boldsymbol{\mathcal{E}} \cdot \mathbf{B} \neq 0$ near the surfaces. As we know, such a field configuration has a nontrivial (anomalous) contribution to the continuity equation for the axial current [7], i.e.,

$$\partial_0 j_5^0 + \boldsymbol{\nabla} \cdot \mathbf{j}_5 = 2im(z)\psi^\dagger \gamma^0 \gamma^5 \psi - \frac{e^2}{4\pi^2}\boldsymbol{\mathcal{E}} \cdot \mathbf{B}. \quad (27)$$

Therefore, it is important to investigate the role of this relation near the surfaces.

Let us assume that the electric field $\boldsymbol{\mathcal{E}}$ is perpendicular to the surface and exists only in a thin layer of depth λ_E. We can conveniently describe such a configuration by using a timelike component of the vector potential, A_0, i.e.,

$$-a - \lambda_E < z < -a: \quad A_0 = -\mathcal{E}z, \quad (28)$$

$$a < z < a + \lambda_E: \quad A_0 = \mathcal{E}z. \quad (29)$$

By assumption, A_0 vanishes inside the slab (i.e., $-a < z < a$), as well as in the vacuum regions outside the thin surface layers (i.e., for $z < -a - \lambda_E$ and $z > a + \lambda_E$).

For the sake of clarity and brevity, we consider the case of zero gap inside the semimetal, $m = 0$. Inside the semimetal, where electric field is absent, the LLL wave function is given by

$$\psi_{-a<z<a} = e^{-iEt}Y_0(\xi)e^{ip_y y}\begin{pmatrix} 0 \\ C_1 e^{-izp_z} \\ 0 \\ C_2 e^{izp_z} \end{pmatrix}. \quad (30)$$

Although the Dirac equation admits exact analytic solutions in constant electric and magnetic fields [60], we find it more convenient and transparent to obtain the corresponding solutions in the region near the slab boundaries, where electric field is present, in the first order of the perturbation theory in electric field $\mathcal{E}$. Since we treat electric field in perturbation theory and only the LLL modes contribute to the axial current in a magnetic field, we begin with the following ansatz [compare with the LLL wave functions (30) in the absence of electric field]:

$$\psi_{\text{vac}} = e^{-iEt}Y_0(\xi)e^{ip_y y}\begin{pmatrix} 0 \\ \phi_1(z) \\ 0 \\ \phi_2(z) \end{pmatrix}. \quad (31)$$

Then the Dirac equation in the region $a < z < a + \lambda_E$ implies the following equations for the functions ϕ_1 and ϕ_2:

$$E\phi_1(z) - v_F(i\partial_z + e\mathcal{E}z/v_F)\phi_1(z) + M\phi_2(z) = 0, \quad (32)$$

$$E\phi_2(z) + v_F(i\partial_z - e\mathcal{E}z/v_F)\phi_2(z) + M\phi_1(z) = 0. \quad (33)$$

We seek solutions of this system of equations as the Taylor series in $\mathcal{E}$ retaining only its two first terms

$$\phi_1(z) = f_0(z) - e\mathcal{E}f_1(z), \quad (34)$$

$$\phi_2(z) = g_0(z) - e\mathcal{E}g_1(z). \quad (35)$$

By substituting Eq. (35) into Eq. (33), we obtain the solutions

$$f_0(z) = A_1 e^{-p'_z z} + A_2 e^{p'_z z},$$

$$g_0(z) = -\frac{1}{M}[A_1 e^{-p'_z z}(E + iv_F p'_z) + A_2 e^{p'_z z}(E - iv_F p'_z)],$$

(36)

$$f_1(z) = \frac{1}{4(v_F p'_z)^3}\Big(A_1 e^{-p'_z z}\big\{i\big(v_F^2 p_z^2 + 2M^2 z\big) - 2E^3 z^2/v_F$$

$$+ E[v_F + 2v_F p'_z z + 2(Mz)^2/v_F] - 2iE^2 z\big\}$$

$$+ A_2 e^{p'_z z}\big\{i\big(v_F^2 p'_z - 2M^2 z\big) + 2E^3 z^2/v_F$$

$$- E[v_F - 2v_F p'_z z + 2(Mz)^2/v_F] + 2iE^2 z\big\}\Big), \quad (37)$$

$$g_1(z) = -\frac{1}{4(v_F p'_z)^3 M}\Big(A_1 e^{-p'_z z}\big\{-2E^3 z^2(E + iv_F p'_z)/v_F$$

$$+ M^2[v_F + 2v_F p'_z z + 2Ez^2(E + iv_F p'_z)/v_F]\big\}$$

$$+ A_2 e^{p'_z z}\big\{2E^3 z^2(E - iv_F p'_z)/v_F$$

$$- M^2[v_F - 2v_F p'_z z + 2Ez^2(E - iv_F p'_z)/v_F]\big\}\Big),$$

(38)

where $p'_z = v_F^{-1}\sqrt{M^2 - E^2}$ and A_1 and A_2 are constants. By matching the wave function (30) and the vacuum functions

$$\psi_{z<-a-\lambda_E} = e^{-iEt}Y_0(\xi)e^{ip_y y}e^{p'_z(z+a+\lambda_E)}C_1''\begin{pmatrix}0\\1\\0\\i\end{pmatrix}, \quad (39)$$

$$\psi_{-a-\lambda_E<z<-a} = e^{-iEt}Y_0(\xi)e^{ip_y y}\begin{pmatrix}0\\f_0(z+a)+e\mathcal{E}f_1(z+a)\\0\\g_0(z+a)+e\mathcal{E}g_1(z+a)\end{pmatrix},$$

(40)

$$\psi_{a<z<a+\lambda_E} = e^{-iEt}Y_0(\xi)e^{ip_y y}\begin{pmatrix}0\\f_0(z-a)-e\mathcal{E}f_1(z-a)\\0\\g_0(z-a)-e\mathcal{E}g_1(z-a)\end{pmatrix},$$

(41)

$$\psi_{z>a+\lambda_E} = e^{-iEt}Y_0(\xi)e^{ip_y y}e^{-p'_z(z-a-\lambda_E)}C_1'\begin{pmatrix}0\\1\\0\\-i\end{pmatrix}, \quad (42)$$

at $z = -a - \lambda_E$, $z = -a$, $z = a - \lambda_E$, and $z = a$, and taking into account the normalization conditions, we find that the linear in $\mathcal{E}$ terms of the wave functions (40) and (41) do not contribute to the continuity equation for axial current because

$$\partial_3\langle j_5^3\rangle_{-a-\lambda_E<z<-a} - 2iM\langle\psi_{-a-\lambda_E<z<-a}^\dagger\gamma^0\gamma^5\psi_{-a-\lambda_E<z<-a}^\dagger\rangle$$

$$= O(e^2\mathcal{E}^2),$$

(43)

$$\partial_3\langle j_5^3\rangle_{a<z<a+\lambda_E} - 2iM\langle\psi_{a<z<a+\lambda_E}^\dagger\gamma^0\gamma^5\psi_{a<z<a+\lambda_E}^\dagger\rangle$$

$$= O(e^2\mathcal{E}^2).$$

(44)

This result is quite natural because the anomalous term in the chiral anomaly is connected with the lack of a chiral symmetry invariant regularization of the famous linearly divergent triangle diagram [7]. Thus, it is high-energy modes whose contribution is divergent and should be regularized which are responsible for the anomalous term in the continuity equation for axial current. Consequently, we conclude that the low-energy modes confined in the semimetal satisfy the continuity equation for axial current without the anomalous term.

VI. CONCLUSION

In this paper, we studied the chiral separation and chiral magnetic effects in a Dirac semimetal with a slab geometry placed in a constant magnetic field perpendicular to its surfaces. We used the Bogolyubov boundary conditions [48] at the surfaces of the slab. It is worth mentioning that such a model was originally used in high-energy physics for the description of hadrons within the framework of the bag models of quarks [54]. This model assumes that the quasiparticles have a large band gap (Dirac mass) in the vacuum regions outside the slab.

Using this model setup, we derived analytically the spectral equation and the wave functions for the bulk modes. Furthermore, we calculated the axial current density and found that, just like in an infinite system, only the LLL modes contribute to this quantity. We show that the main consequence of a finite slab thickness is that the axial current density becomes quantized. The corresponding quantization could be revealed in its functional dependence on the chemical potential and the thickness of the slab. The underlying reason for the quantization is the discretization of the wave vectors and energy levels in the slab. In other words, the axial current density originates from helicity-correlated standing waves, associated with the LLL. It is also interesting to point that there is no chiral charge accumulation on the semimetal boundaries, as might have been naively expected. The size of the quantization steps in the axial current density as a function of the chemical potential, see Fig. 1, is given by $\delta\langle j_5^3\rangle = eBv_F/(4a\pi)$. Because the steps are inversely proportional to the thickness of the slab a, most likely the corresponding structure can be observed in experiment only if the samples are sufficiently thin.

As we show in this study, the dependence of the axial current density on the thickness of the slab a has a very characteristic sawtooth shape; see Fig. 2. With increasing the value of a, the quantization effects become less pronounced and the axial current density gradually approaches the limit of an infinite system. Interestingly, the quantization persists even in the case of Dirac quasiparticles with nonzero gaps. However, a nonzero gap has a damping effect in the dependence on a.

We also find that, in the case of gapped Dirac fermions, $m \neq 0$, the axial current density is not uniform across the semimetal slab, but oscillates as a function of the position; see Fig. 3. This is in contrast to the chiral limit when the axial current is constant. In fact, the larger is the gap, the more pronounced are the oscillations. Formally, such a behavior is connected with a nonconservation of the axial charge. It appears that the amplitude of the oscillations decreases with increasing the distance from the boundaries. To the best of

our knowledge, the possibility of such oscillations and their key features have not been reported before. It would be very interesting to test this scenario in the lattice simulations. Also, this phenomenon could potentially be investigated experimentally in a semimetal with a spontaneously generated gap, e.g., via magnetic catalysis [61], or another mechanism.

By introducing a nonzero chiral chemical potential μ_5, we also analyzed the chiral magnetic effect in a semimetal slab. In contrast to the axial current density due to the CSE, the corresponding electric current due to the CME is absent in a semimetal slab. In retrospect, the vanishing result is a natural outcome of the nonanomalous continuity equation for the electric current and the Bogolyubov boundary conditions [54]. Indeed, the latter are equivalent to the requirement of vanishing electric current from the semimetal to vacuum. It is worth emphasizing, however, that in this study we limited our consideration only to static configurations. This automatically excludes all transient phenomena in which nonzero electric currents are generated out of equilibrium and evolve in time. The corresponding generation of the CME in finite-size samples would be very interesting and should be studied in the future. Such a problem is beyond the scope of this study however.

We took into account a nonzero electric field near the slab surface created by a double charge layer present at the surfaces of solids. It was found that, because of the presence of this electric field, the continuity equation for the axial current is fulfilled for the low-energy modes considered in this study without taking into account the linear in electric field anomalous term. In all fairness, the current understanding of the chiral anomaly in the problem of a finite-size Dirac semimetal remains incomplete. While it is understood that the chiral symmetry is explicitly broken by the surface effects, it is not completely clear whether the model implementation of the boundary layer used in the present study is sufficient to capture all relevant physics effects.

One of the limitations of this study is the use of a special orientation of the magnetic field perpendicular to the slab surfaces. The main reason for this was that the analysis would become much more challenging in the case of a tilted magnetic field. From the physics viewpoint, the complications come from the need of squeezing the Landau orbits into a finite thickness of the slab. Nevertheless, here we could speculate that, in the case of a general orientation of the magnetic field, one may consider separately the perpendicular and parallel (with respect to the surface) components of the currents, while the results for the perpendicular components of the currents are expected to remain qualitatively the same as in the special case considered in this paper (except for the replacement $B \to B\cos\theta$, where θ is an angle between the direction of the magnetic field and the normal to the slab surface). The parallel components of the currents are most likely to be the same as in an unbounded infinite system, but with $B \to B\sin\theta$. While plausible, such a scenario clearly requires a further in-depth investigation, which is beyond the scope of this study.

APPENDIX A: DERIVATION OF THE LANDAU-LEVEL WAVE FUNCTIONS

In this Appendix we derive the Landau-level wave functions in the model described by the Hamiltonian in Eq. (1). We look for the solutions of the Dirac equation, $H\psi(\mathbf{r}) = E\psi(\mathbf{r})$, in the form $\psi(\mathbf{r}) = e^{ip_z z + ip_y y}\phi(x)$. In this case, function $\phi(x)$ satisfies the following equation:

$$[(-v_F p_z \gamma^z - v_F p_y \gamma^y + i v_F \gamma^x \partial_x)\gamma^0$$
$$- v_F eBx\gamma^y\gamma^0 + m\gamma^0]\phi(x) = E\phi(x). \quad \text{(A1)}$$

In the case of a constant magnetic field in the $+z$ direction, assumed here, we choose the vector potential in the Landau gauge, $\mathbf{A} = (0, Bx, 0)$. (Clearly, all observables should be independent of a specific gauge choice.) Instead of the x coordinate, it is convenient to introduce a new dimensionless variable,

$$\xi = \sqrt{|eB|}\left(\frac{p_y}{eB} + x\right), \quad \text{(A2)}$$

and rewrite Eq. (A1) as follows:

$$\left[\partial_\xi + is_\perp\xi\gamma^y\gamma^x - \frac{i\gamma^x}{\sqrt{|eB|}}\right.$$
$$\left.\times[p_z\gamma^z + (m/v_F) - (E/v_F)\gamma^0]\right]\phi(\xi) = 0, \quad \text{(A3)}$$

where $s_\perp = \text{sgn}(eB)$. By making use of the same approach as in Ref. [55], let us introduce a set of linearly independent bispinors $u_s^\pm$ that satisfy the following relations:

$$i\gamma^y\gamma^x u_s^\pm = \mp u_s^\pm, \quad \text{(A4)}$$

$$\gamma^y\gamma^x(E\gamma^0 - v_F p_z\gamma^z)u_s^\pm = s\sqrt{v_F^2 p_z^2 - E^2}\, u_s^\pm, \quad \text{(A5)}$$

$$\frac{\gamma^x(\gamma^0 E - \gamma^z v_F p_z - m)}{\sqrt{E^2 - v_F^2 p_z^2 - m^2}}\, u_s^- = u_s^+. \quad \text{(A6)}$$

Then, by expressing the wave function $\phi(\xi)$ as a linear combination of the two bispinors,

$$\phi_s(\xi) = \Phi_+^s(\xi)u_s^+ + \Phi_-^s(\xi)u_s^-, \quad \text{(A7)}$$

and using the relations in Eqs. (A4) through (A6), we rewrite the equation for the wave function (A3) in the following form:

$$[\partial_\xi\Phi_\pm^s(\xi) \mp s_\perp\xi\Phi_\pm^s(\xi) + i\kappa\Phi_\mp^s(\xi)] = 0,$$
$$\left[\partial_\xi^2 \mp s_\perp - \xi^2 + \kappa^2\right]\Phi_\pm^s(\xi) = 0, \quad \text{(A8)}$$

where $\kappa = \sqrt{E^2 - v_F^2 p_z^2 - m^2}/\epsilon_L$ and $\epsilon_L \equiv v_F\sqrt{|eB|}$. Without loss of generality, let us choose $s_\perp \equiv \text{sgn}(eB) = +1$. Then, the solutions of Eq. (A8) are given in terms of the

parabolic cylinder functions [62]:

$$\Phi^s_-(\xi) = D_{\kappa^2/2}(\sqrt{2}\xi), \quad \Phi^s_+(\xi) = \frac{i\kappa}{\sqrt{2}} D_{\kappa^2/2-1}(\sqrt{2}\xi). \tag{A9}$$

By requiring that the wave functions are finite at $|\xi| \to \infty$, one finds that $\kappa^2/2 = n$ where $n = 0,1,2,\ldots$ are nonnegative integers. In this special case, the parabolic cylinder functions $D_n(\sqrt{2}\xi)$ can be expressed in terms of the Hermite polynomials $H_n(\xi)$: $D_n(\sqrt{2}\xi) = \frac{1}{\sqrt{2^n}}e^{-\xi^2/2}H_n(\xi)$. By making use of the definition of κ, we also obtain the corresponding Landau-level energies: $E_n^2 = v_F^2 p_z^2 + m^2 + 2n\epsilon_L^2$. It should be noted that function $\Phi^s_+(\xi)$ is not finite at $|\xi| \to \infty$ when $n = 0$. However, by using the relation in Eq. (A6), we can express u_s^+ through u_s^-, i.e.,

$$\begin{aligned}
u_s^+ &= \frac{-m\gamma^x - \gamma^y s\sqrt{v_F^2 p_z^2 - E_n^2}}{\sqrt{E_n^2 - v_F^2 p_z^2 - m^2}} u_s^- \\
&= -\gamma^x \frac{m + s\sqrt{E_n^2 - v_F^2 p_z^2}}{\sqrt{E_n^2 - v_F^2 p_z^2 - m^2}} u_s^-.
\end{aligned} \tag{A10}$$

Then, in the case of the LLL ($n = 0$), we see that the coefficient in the last equation vanishes if $s = -1$. This means that, for the LLL, only one value of the spin, $s = -1$, is allowed. For the higher Landau levels, both spin projections, i.e., $s = \pm 1$, are allowed. The Landau-level wave functions are given by

$$\begin{aligned}
\phi_s(\xi) = &\left[\frac{e^{-\xi^2/2}}{\sqrt{2^n}}H_n(\xi) - i\gamma^x \frac{m + s\sqrt{m^2 + 2n\epsilon_L^2}}{\sqrt{2\epsilon_L^2}}\right. \\
&\left. \times \frac{e^{-\xi^2/2}}{\sqrt{2^{n-1}}}H_{n-1}(\xi)\right] u_s^-,
\end{aligned} \tag{A11}$$

where, according to Eqs. (A4) through (A6),

$$u_s^- = \begin{pmatrix} 0 \\ \chi_2 \\ 0 \\ \chi_4 \end{pmatrix}, \quad u_s^+ = \frac{m + s\sqrt{E_n^2 - v_F^2 p_z^2}}{\sqrt{E_n^2 - v_F^2 p_z^2 - m^2}}\begin{pmatrix} -\chi_4 \\ 0 \\ \chi_2 \\ 0 \end{pmatrix},$$

$$\chi_4 = \frac{s\sqrt{E_n^2 - v_F^2 p_z^2}}{E_n - v_F p_z}\chi_2. \tag{A12}$$

Finally, the explicit form of the Landau-level wave functions reads

$$\psi(\mathbf{r})_{n=0} = C_0 e^{ip_z z + ip_y y} \phi_{0;s=-1}(\xi), \tag{A13}$$

$$\psi(\mathbf{r})_{n\neq 0} = e^{ip_z z + ip_y y}[C_1\phi_{n;s=+1}(\xi) + C_2\phi_{n;s=-1}(\xi)], \tag{A14}$$

where

$$\phi(\xi)_{n>0,s=+1} = C_1 \begin{pmatrix} -i\frac{\sqrt{m^2+2n\epsilon_L^2}}{E_n-v_F p_z}\frac{m+\sqrt{m^2+2n\epsilon_L^2}}{\sqrt{2n\epsilon_L^2}}Y_{n-1}(\xi) \\ Y_n(\xi) \\ i\frac{m+\sqrt{m^2+2n\epsilon_L^2}}{\sqrt{2n\epsilon_L^2}}Y_{n-1}(\xi) \\ \frac{\sqrt{m^2+2n\epsilon_L^2}}{E_n-v_F p_z}Y_n(\xi) \end{pmatrix}, \tag{A15}$$

$$\phi(\xi)_{n>0,s=-1} = C_2 \begin{pmatrix} i\frac{\sqrt{m^2+2n\epsilon_L^2}}{E_n-v_F p_z}\frac{m-\sqrt{m^2+2n\epsilon_L^2}}{\sqrt{2n\epsilon_L^2}}Y_{n-1}(\xi) \\ Y_n(\xi) \\ i\frac{m-\sqrt{m^2+2n\epsilon_L^2}}{\sqrt{2n\epsilon_L^2}}Y_{n-1}(\xi) \\ -\frac{\sqrt{m^2+2n\epsilon_L^2}}{E_n-v_F p_z}Y_n(\xi) \end{pmatrix}, \tag{A16}$$

$$\phi(\xi)_{n=0,s=-1} = C_0 \begin{pmatrix} 0 \\ Y_0(\xi) \\ 0 \\ -\frac{m}{E_0-v_F p_z}Y_0(\xi) \end{pmatrix}. \tag{A17}$$

Here $Y_n(\xi) = \frac{e^{-\xi^2/2}}{\sqrt{2^n n!\sqrt{\pi}}}H_n(\xi)$ are the harmonic oscillator wave functions. By making use of Eqs. (A13) through (A17), it is straightforward to obtain the wave functions (3) and (4) in the main text.

APPENDIX B: MATCHING SOLUTIONS AT THE SEMIMETAL BOUNDARIES

In this Appendix, we derive the explicit expressions for the wave functions in the semimetal with a slab geometry by matching the general solutions, presented in Eqs. (5) and (6) in the main text, with the corresponding vacuum solutions. This is done by making use of the Bogolyubov bag model, in which the wave functions outside the semimetal satisfy the same type Dirac equation, but with a large vacuum band gap M.

1. Matching the wave functions of the $n = 0$ modes

Let us first consider the $n = 0$ modes. In order to obtain normalizable solutions outside the semimetal, in the regions with $z > a$ and $z < -a$, in Eq. (3) we will replace p_z with ip'_z and $-ip'_z$, respectively. With such a parametrization of the vacuum solutions, the energy of the $n = 0$ modes is given by $E = \pm\sqrt{M^2 - (v_F p'_z)^2}$. In the limit $M \to \infty$, the corresponding solutions must have the same (finite) energy as the $n = 0$ modes in the bulk. This implies that $v_F p'_z \approx M - (m^2 + v_F^2 p_z^2)/(2M)$. Therefore, to leading order in the inverse powers of M, the corresponding wave functions in the

vacuum are given by

$$\psi(\mathbf{r})_{n=0,z>a} = C'_0 Y_0(\xi) e^{ip_y y} e^{-M(z-a)/v_F} \begin{pmatrix} 0 \\ 1 \\ 0 \\ -i \end{pmatrix}, \quad (B1)$$

$$\psi(\mathbf{r})_{n=0,z<-a} = C''_0 Y_0(\xi) e^{ip_y y} e^{M(z+a)/v_F} \begin{pmatrix} 0 \\ 1 \\ 0 \\ i \end{pmatrix}. \quad (B2)$$

By making use of Eqs. (5), (B1), and (B2), we find that the matching conditions on the two sides of the semimetal slab,

$$\Psi_{\text{slab}}(x,y,a)_{n=0} = \psi(x,y,a)_{n=0,z>a}, \quad (B3)$$

$$\Psi_{\text{slab}}(x,y,-a)_{n=0} = \psi(x,y,-a)_{n=0,z<-a}, \quad (B4)$$

lead to the following equation for p_z:

$$v_F p_z \cos(2ap_z) + m \sin(2ap_z) = 0, \quad (B5)$$

where $p_z \neq 0$. Note that $p_z = 0$ is not allowed because it corresponds to a trivial solution for the wave function.

Satisfying the boundary conditions also fixes the value of constant $\tilde{C}_0$ in the superposition of two counterpropagating waves in the bulk solution (5):

$$\tilde{C}_0 = -e^{2ip_z a} C_0 \frac{E_0(E_0 + v_F p_z)}{m(m - i v_F p_z)}. \quad (B6)$$

By taking this into account, we derive the following final expression for the wave function inside the semimetal:

$$\Psi_{\text{slab}}(\mathbf{r})_{n=0} = C_0 Y_0(\xi) e^{ip_y y}$$

$$\times \begin{pmatrix} 0 \\ 2e^{iap_z} \frac{v_F p_z \cos[p_z(z-a)] - (m+iE_0)\sin[p_z(z-a)]}{im + v_F p_z - E_0} \\ 0 \\ -2i e^{iap_z} \frac{v_F p_z \cos[p_z(z-a)] - (m-iE_0)\sin[p_z(z-a)]}{im + v_F p_z - E_0} \end{pmatrix}, \quad (B7)$$

where

$$|C_0|^2 = \frac{\epsilon_L[m^2 + v_F p_z(v_F p_z - E_0)]}{4v_F[2a(m^2 + v_F^2 p_z^2) + m v_F]} \quad (B8)$$

is obtained from the condition of the wave function normalization.

2. Matching the wave functions of $n > 0$ modes

Let us now consider the modes with $n > 0$ outside the slab. As in the case of the $n = 0$ mode, in order to obtain normalizable solutions in the $z > a$ and $z < -a$ regions, in Eq. (4) we replace p_z with ip'_z and $-ip'_z$, respectively. The energies of such solutions are given by $E_n = \pm\sqrt{M^2 + 2n\epsilon_L^2 - (v_F p'_z)^2}$. In the limit $M \to \infty$, these should coincide with the corresponding expressions for the Landau-level energies in the bulk. This is satisfied if we choose $v_F p'_z \approx M - (m^2 + v_F^2 p_z^2)/(2M)$ in the vacuum solutions. By taking this into account, we derive the following vacuum wave function in the $z > a$ region:

$$\psi(\mathbf{r})_{n,z>a} = e^{-p'_z(z-a)+ip_y y}\left[M(C'_+ + C'_-)\frac{Y_{n-1}(\xi)}{\sqrt{2n\epsilon_L^2}} \begin{pmatrix} 1 \\ 0 \\ i \\ 0 \end{pmatrix} + \begin{pmatrix} -iE_n(C'_+ + C'_-)\frac{Y_{n-1}(\xi)}{\sqrt{2n\epsilon_L^2}} \\ C'_+ Y_n(\xi) \\ 0 \\ iC'_- Y_n(\xi) \end{pmatrix} + O\left(\frac{1}{M}\right) \right], \quad (B9)$$

where we kept terms up to subleading order in the inverse powers of M. From the normalization of the wave function (B9), we find that

$$C'_\pm = C'_1 \frac{\sqrt{2n\epsilon_L^2}}{2M} \pm C'_2 + O\left(\frac{1}{M^2}\right). \quad (B10)$$

Therefore, the final expression for the wave function in the vacuum region $z > a$ is given by

$$\psi(\mathbf{r})_{n,z>a} = e^{-M(z-a)/v_F + ip_y y}\left[C'_1 Y_{n-1}(\xi) \begin{pmatrix} 1 \\ 0 \\ i \\ 0 \end{pmatrix} + C'_2 Y_n(\xi) \begin{pmatrix} 0 \\ 1 \\ 0 \\ -i \end{pmatrix} \right]. \quad (B11)$$

The wave function in the other vacuum region, $z < -a$, can be obtained in a similar way. The final result reads

$$\psi(\mathbf{r})_{n,z<-a} = e^{M(z+a)/v_F + ip_y y}\left[C''_1 Y_{n-1}(\xi) \begin{pmatrix} -1 \\ 0 \\ i \\ 0 \end{pmatrix} + C''_2 Y_n(\xi) \begin{pmatrix} 0 \\ 1 \\ 0 \\ i \end{pmatrix} \right]. \quad (B12)$$

The matching conditions at the boundary of the semimetal are similar to those in Eqs. (B3) and (B4), i.e.,

$$\Psi_{\text{slab}}(x,y,a)_{n>0} = \psi(x,y,a)_{n>0,z>a}, \quad (B13)$$

$$\Psi_{\text{slab}}(x,y,-a)_{n>0} = \psi(x,y,-a)_{n>0,z<-a}. \quad (B14)$$

By substituting the wave functions from Eqs. (6), (B11), and (B12) into these matching conditions, we find that p_z should satisfy the same spectral equation (B5) as in the case of the $n = 0$ modes. By taking into account, however, that the rank of the system of Eqs. (B13) and (B14) is 2 units less than the dimension of the system, we obtain the following two linearly independent solutions for each higher Landau level ($n > 0$) inside the slab:

$$\Psi^{(1)}_{\text{slab}}(\mathbf{r})_{n>0} = C_+ e^{ip_y y} \begin{pmatrix} -2i \frac{\sqrt{2n\epsilon_L^2} e^{-ip_z a} \sin[p_z(z+a)]}{m+i(v_F p_z - E_n)} Y_{n-1}(\xi) \\ 2i e^{-iap_z} \frac{v_F p_z \cos[p_z(z+a)] + (m - iE_n)\sin[p_z(z+a)]}{m+i(v_F p_z - E_n)} Y_n(\xi) \\ \frac{\sqrt{2n\epsilon_L^2} e^{-ip_z a}[m + i(v_F p_z + E_n)]\sin[p_z(z+a)]}{m^2 + iv_F p_z m + 2n\epsilon_L^2} Y_{n-1}(\xi) \\ -2 e^{-iap_z} \frac{v_F p_z \cos[p_z(z+a)] + (m + iE_n)\sin[p_z(z+a)]}{m+i(v_F p_z - E_n)} Y_n(\xi) \end{pmatrix}, \tag{B15}$$

$$\Psi^{(2)}_{\text{slab}}(\mathbf{r})_{n>0} = C_- e^{ip_y y} \begin{pmatrix} 2 e^{-iap_z} \frac{i[m^2 - im(v_F p_z + E_n)]\sin[p_z(z+a)] + 2n\epsilon_L^2 \cos[p_z(z+a)] + v_F p_z[v_F p_z + E_n]e^{ip_z(z+a)}}{\sqrt{2n\epsilon_L^2}\sqrt{m^2 + 2n\epsilon_L^2}} Y_{n-1}(\xi) \\ -2 \frac{e^{-ip_z a}(v_F p_z + E_n)\sin[p_z(z+a)]}{\sqrt{m^2 + 2n\epsilon_L^2}} Y_n(\xi) \\ 2i \frac{e^{-iap_z}\sqrt{m^2 + 2n\epsilon_L^2}\{p_z \cos[p_z(z+a)] + (m - iE_n)\sin[p_z(z+a)]\}}{\sqrt{2n\epsilon_L^2}(v_F p_z - E_n)} Y_{n-1}(\xi) \\ 2i e^{-iap_z} \frac{(v_F p_z + E_n)\sin[p_z(z+a)]}{\sqrt{m^2 + 2n\epsilon_L^2}} Y_n(\xi) \end{pmatrix}, \tag{B16}$$

where the normalization constants are given by

$$|C_+|^2 = \frac{\epsilon_L p_z [m^2 + n\epsilon_L^2 + v_F p_z(v_F p_z - E_n)]}{4v_F [2ap_z E_n^2 + mv_F p_z - n\epsilon_L^2 \sin(4ap_z)]}, \tag{B17}$$

$$|C_-|^2 = \frac{n\epsilon_L^3 p_z(v_F p_z - E_n)^2}{4v_F (m^2 + 2n\epsilon_L^2)[2ap_z E_n^2 + mv_F p_z - n\epsilon_L^2 \sin(4ap_z)]}. \tag{B18}$$

3. Matching of the LLL wave functions in the case of finite vacuum gap

Let us now consider the LLL in the case of large but finite vacuum gap M. In order to derive the tails of the LLL wave functions in the regions $z > a$ and $z < -a$ outside the slab, we use Eq. (3) with p_z replaced with ip_z' and $-ip_z'$, respectively, i.e.,

$$\psi(\mathbf{r})_{n=0, z>a} = Y_0(\xi) e^{ip_y y} e^{-p_z'(z-a)} A_0' \begin{pmatrix} 0 \\ 1 \\ 0 \\ -\frac{M}{E_0 - iv_F p_z'} \end{pmatrix}, \tag{B19}$$

$$\psi(\mathbf{r})_{n=0, z<-a} = Y_0(\xi) e^{ip_y y} e^{p_z'(z+a)} A_0'' \begin{pmatrix} 0 \\ 1 \\ 0 \\ -\frac{M}{E_0 + iv_F p_z'} \end{pmatrix}. \tag{B20}$$

Here $p_z' = v_F^{-1}\sqrt{M^2 - E_0^2}$. Enforcing the matching conditions at the boundaries of the slab, see Eqs. (B3) and (B4), we find that the wave vector p_z should satisfy the following spectral equation:

$$\frac{-v_F p_z \sqrt{M^2 - E_0^2} \cos(2ap_z) + (E_0^2 - mM)\sin(2ap_z)}{M} = 0. \tag{B21}$$

[As expected, in the limit $M \to \infty$, this equation reduces to Eq. (B5).] The corresponding LLL wave functions inside the semimetal and outside the slab are given by

$$\Psi_{\text{slab}}(\mathbf{r})_{n=0} = A_0 Y_0(\xi) e^{ip_y y} \begin{pmatrix} 0 \\ e^{ip_z(z-a)} - e^{-ip_z(z-a)} \frac{(E_0 + v_F p_z)[E_0^2 - mM - iv_F p_z\sqrt{M^2 - E_0^2}]}{mE_0(m-M)} \\ 0 \\ \frac{m}{v_F p_z - E_0}\left[e^{ip_z(z-a)} - e^{-ip_z(z-a)} \frac{(E_0 - v_F p_z)[E_0^2 - mM - iv_F p_z\sqrt{M^2 - E_0^2}]}{mE_0(m-M)} \right] \end{pmatrix}, \tag{B22}$$

$$\psi(\mathbf{r})_{n=0,z>a} = -A_0 Y_0(\xi) e^{i p_y y} e^{-\sqrt{M^2 - E_0^2}(z-a)/v_F} \frac{v_F p_z \left[m(m-M) + (v_F p_z + E_0)(v_F p_z - i\sqrt{M^2 - E_0^2}) \right]}{m E_0 (m-M)} \begin{pmatrix} 0 \\ 1 \\ 0 \\ -\frac{M}{E_0 - i\sqrt{M^2 - E_0^2}} \end{pmatrix},$$

(B23)

$$\psi(\mathbf{r})_{n=0,z<-a} = -2A_0 Y_0(\xi) e^{i p_y y} e^{\sqrt{M^2 - E_0^2}(z+a)/v_F} \frac{E_0 m \left[v_F p_z \cos(2a p_z) + \sqrt{M^2 - E_0^2} \sin(2a p_z) \right]}{(E_0 - v_F p_z)\left[m(E_0 - i\sqrt{M^2 - E_0^2}) - M(v_F p_z + E_0) \right]} \begin{pmatrix} 0 \\ 1 \\ 0 \\ -\frac{M}{E_0 + i\sqrt{M^2 - E_0^2}} \end{pmatrix},$$

(B24)

where the overall constant A_0 is obtained from the normalization condition. Its explicit expression is given by

$$|A_0|^2 = \frac{\epsilon_L (m-M) E_0 (E_0 - v_F p_z)}{4 v_F \left(2a E_0^2 (m-M) - m v_F \sqrt{M^2 - E_0^2} - \frac{v_F^3 p_z^2 M}{\sqrt{M^2 - E_0^2}} \right)}.$$

(B25)

[1] S. Borisenko, Q. Gibson, D. Evtushinsky, V. Zabolotnyy, B. Buchner, and R. J. Cava, Phys. Rev. Lett. **113**, 027603 (2014).

[2] M. Neupane, S.-Y. Xu, R. Sankar, N. Alidoust, G. Bian, C. Liu, I. Belopolski, T.-R. Chang, H.-T. Jeng, H. Lin, A. Bansil, F. Chou, and M. Z. Hasan, Nat. Commun. **5**, 3786 (2014).

[3] Z. K. Liu, B. Zhou, Y. Zhang, Z. J. Wang, H. M. Weng, D. Prabhakaran, S.-K. Mo, Z. X. Shen, Z. Fang, X. Dai, Z. Hussain, and Y. L. Chen, Science **343**, 864 (2014).

[4] A. M. Turner and A. Vishwanath, arXiv:1301.0330.

[5] O. Vafek and A. Vishwanath, Annu. Rev. Condens. Matter Phys. **5**, 83 (2014).

[6] A. A. Burkov, J. Phys.: Condens. Matter **27**, 113201 (2015).

[7] S. L. Adler, Phys. Rev. **177**, 2426 (1969); J. S. Bell and R. Jackiw, Nuovo Cimento A **60**, 47 (1969).

[8] H. B. Nielsen and M. Ninomiya, Phys. Lett. B **130**, 389 (1983).

[9] H. Weng, C. Fang, Z. Fang, A. Bernevig, and X. Dai, Phys. Rev. X **5**, 011029 (2015).

[10] S.-M. Huang, Su-Y. Xu, I. Belopolski, C.-C. Lee, G. Chang, B. Wang, N. Alidoust, G. Bian, M. Neupane, A. Bansil, H. Lin, and M. Z. Hasan, Nat. Commun. **6**, 7373 (2015).

[11] C. Zhang, Z. Yuan, S. Xu, Z. Lin, B. Tong, M. Z. Hasan, J. Wang, C. Zhang, and S. Jia, arXiv:1502.00251.

[12] S.-Y. Xu, I. Belopolski, N. Alidoust, M. Neupane, C. Zhang, R. Sankar, S.-M. Huang, C.-C. Lee, G. Chang, B. Wang, G. Bian, H. Zheng, D. S. Sanchez, F. Chou, H. Lin, S. Jia, and M. Z. Hasan, Science **349**, 613 (2015).

[13] B. Q. Lv, H. M. Weng, B. B. Fu, X. P. Wang, H. Miao, J. Ma, P. Richard, X. C. Huang, L. X. Zhao, G. F. Chen, Z. Fang, X. Dai, T. Qian, and H. Ding, Phys. Rev. X **5**, 031013 (2015).

[14] X. Huang, L. Zhao, Y. Long, P. Wang, D. Chen, Z. Yang, H. Liang, M. Xue, H. Weng, Z. Fang, X. Dai, and G. Chen, Phys. Rev. X **5**, 031023 (2015).

[15] S.-Y. Xu, N. Alidoust, I. Belopolski, C. Zhang, G. Bian, T.-R. Chang, H. Zheng, V. Strokov, D. S. Sanchez, G. Chang, Z. Yuan, D. Mou, Y. Wu, L. Huang, C.-C. Lee, S.-M. Huang, B. K. Wang, A. Bansil, H.-T. Jeng, T. Neupert, A. Kaminski, H. Lin, S. Jia, and M. Z. Hasan, Nat. Phys. **11**, 748 (2015).

[16] K. Fukushima, D. E. Kharzeev, and H. J. Warringa, Phys. Rev. D **78**, 074033 (2008).

[17] D. Kharzeev and A. Zhitnitsky, Nucl. Phys. A **797**, 67 (2007).

[18] D. E. Kharzeev, L. D. McLerran, and H. J. Warringa, Nucl. Phys. A **803**, 227 (2008).

[19] A. A. Burkov and L. Balents, Phys. Rev. Lett. **107**, 127205 (2011).

[20] A. A. Burkov, M. D. Hook, and L. Balents, Phys. Rev. B **84**, 235126 (2011).

[21] A. A. Zyuzin and A. A. Burkov, Phys. Rev. B **86**, 115133 (2012).

[22] M. M. Vazifeh and M. Franz, Phys. Rev. Lett. **111**, 027201 (2013).

[23] B. I. Abelev et al. (STAR Collaboration), Phys. Rev. Lett. **103**, 251601 (2009); Phys. Rev. C **81**, 054908 (2010).

[24] G. Wang (STAR Collaboration), Nucl. Phys. A **904-905**, 248c (2013).

[25] H. Ke (STAR Collaboration), J. Phys.: Conf. Ser. **389**, 012035 (2012).

[26] L. Adamczyk et al. (STAR Collaboration), Phys. Rev. C **89**, 044908 (2014).

[27] L. Adamczyk et al. (STAR Collaboration), Phys. Rev. Lett. **114**, 252302 (2015).

[28] I. Selyuzhenkov (ALICE Collaboration), Prog. Theor. Phys. Suppl. **193**, 153 (2012).

[29] S. A. Voloshin, Phys. Rev. C **70**, 057901 (2004).

[30] D. E. Kharzeev, Ann. Phys. **325**, 205 (2010); K. Fukushima, D. E. Kharzeev, and H. J. Warringa, Nucl. Phys. A **836**, 311 (2010).

[31] J. Liao, Pramana **84**, 901 (2015).

[32] D. E. Kharzeev, Annu. Rev. Nucl. Part. Sci. **65**, 193 (2015).

[33] X.-G. Huang, arXiv:1509.04073.

[34] Q. Li, D. E. Kharzeev, C. Zhang, Y. Huang, I. Pletikosic, A. V. Fedorov, R. D. Zhong, J. A. Schneeloch, G. D. Gu, and T. Valla, arXiv:1412.6543.

[35] A. Vilenkin, Phys. Rev. D **22**, 3067 (1980).

[36] M. A. Metlitski and A. R. Zhitnitsky, Phys. Rev. D **72**, 045011 (2005).

[37] G. M. Newman and D. T. Son, Phys. Rev. D **73**, 045006 (2006).

[38] E. V. Gorbar, V. A. Miransky, and I. A. Shovkovy, Phys. Rev. D **83**, 085003 (2011).

[39] Y. Burnier, D. E. Kharzeev, J. Liao, and H.-U. Yee, Phys. Rev. Lett. **107**, 052303 (2011).

[40] G. Basar and G. V. Dunne, Lect. Notes Phys. **871**, 261 (2013).

[41] J. Ambjorn, J. Greensite, and C. Peterson, Nucl. Phys. B **221**, 381 (1983); N. Sadooghi and A. J. Salim, Phys. Rev. D **74**, 085032 (2006).

[42] E. V. Gorbar, V. A. Miransky, and I. A. Shovkovy, Phys. Rev. C **80**, 032801(R) (2009).

[43] K. Fukushima and M. Ruggieri, Phys. Rev. D **82**, 054001 (2010).

[44] E. V. Gorbar, V. A. Miransky, and I. A. Shovkovy, Phys. Lett. B **695**, 354 (2011).

[45] E. V. Gorbar, V. A. Miransky, and I. A. Shovkovy, Phys. Rev. B **88**, 165105 (2013).

[46] S. Ebihara, K. Fukushima, and T. Oka, arXiv:1509.03673.

[47] C. K. Chan, P. A. Lee, K. S. Burch, J. H. Han, and Y. Ran, arXiv:1509.05400.

[48] P. N. Bogolioubov, Ann. Inst. Henri Poincare **8**, 163 (1967).

[49] A. R. Akhmerov and C. W. J. Beenakker, Phys. Rev. Lett. **98**, 157003 (2007).

[50] P. Recher, B. Trauzettel, A. Rycerz, Ya. M. Blanter, C. W. J. Beenakker, and A. F. Morpurgo, Phys. Rev. B **76**, 235404 (2007).

[51] M. I. Katsnelson, K. S. Novoselov, and A. K. Geim, Nat. Phys. **2**, 620 (2006).

[52] B. Lenoir, M. Cassart, J.-P. Michenaud, H. Scherrer, and S. Scherrer, J. Phys. Chem. Solids **57**, 89 (1996).

[53] J. C. Y. Teo, L. Fu, and C. L. Kane, Phys. Rev. B **78**, 045426 (2008).

[54] A. W. Thomas, in *Advances in Nuclear Physics*, edited by J. W. Negele and E. Vogt, Vol. 13 (Plenum Press, New York, 1984), pp. 1-137.

[55] A. I. Akhiezer and V. B. Berestetskii, *Quantum Electrodynamics* (Interscience, New York, 1965).

[56] J.-H. Zhou, H. Jiang, Q. Niu, and J.-R. Shi, Chin. Phys. Lett. **30**, 027101 (2013).

[57] G. Basar, D. E. Kharzeev, and H.-U. Yee, Phys. Rev. B **89**, 035142 (2014).

[58] K. Landsteiner, Phys. Rev. B **89**, 075124 (2014).

[59] J. A. Venables, *Introduction to Surface and Thin-Film Processes* (Cambridge University Press, Cambridge, 2000).

[60] V. G. Bagrov and D. M. Gitman, *The Dirac Equation and Its Solutions* (De Gruyter, Berlin, 2014).

[61] V. P. Gusynin, V. A. Miransky, and I. A. Shovkovy, Phys. Lett. B **349**, 477 (1995); Nucl. Phys. B **462**, 249 (1996); for a review, see V. A. Miransky and I. A. Shovkovy, Phys. Rep. **576**, 1 (2015).

[62] H. Bateman and A. Erdelyi, *Higher Transcendental Functions*, Vol. 2 (McGraw-Hill Book Company, New York, 1953).